TABLE 1 Comparison between characteristics of the proposed antenna and three previously reported MTM antennas

Performance characteristics	Antenna reported in this paper	Antenna reported in Ref. [6]	Antenna reported in Ref. [2]	Antenna reported in Ref. [7]
L × W × H (cm × cm × cm)	8 × 8 × 1.1	9.3 × 9.3 × 2	3.3 × 4.6 × 1.1	1.8 × 1 × 0.8
Resonant frequency (MHz)	590	250	615	2450
$|S_{11}|$ (at resonant) (dB)	−14.3	−11.9	−17	−18
Gain (dB)	−2.2	−3.9	−3.4	−3
BW (−10 dB) (%)	1.7	1	2.1	2
Directivity (dB)	3.47	3. 4	Not reported	Not reported
Axial ratio (dB)	−14	−12	Not reported	Not reported
Efficiency (%)	27.1	19.8	Not reported	Not reported
Miniaturization factor	3.1	6.45	3.3	5.3

4 | CONCLUSION

A circular spiral-based MTM was investigated and its electromagnetic parameters were retrieved. The manufactured MTM was used as the patch antenna substrate. Electromagnetic characteristics of the MTM antenna were measured. The gain of the proposed antenna is −2.2 dB which shows significant enhancement over the −3.9 dB reported in Ref. [6]. The 1.7% bandwidth of proposed MTM antenna is also acceptable in patch antenna applications and comparable to previous works. It should be noticed that the new design for the arrangement of MTM strips applied in this paper, resulted in a light profile antenna (about 1/6) relative to previously reported MTM antennas in which their substrates were occupied by a host dielectric material.

REFERENCES

[1] Engheta N, Ziolkowski RW. *Metamaterials, Physics and Engineering Explorations*. John Wiley & Sons; Hoboken, NJ, 2006.

[2] Yousefi L, Ramahi O. Miniaturised antennas using artificial magnetic materials with fractal Hilbert inclusions. *Electron Lett.* 2010; 46:816–817.

[3] BuellMosallaei KH, Sarabandi K. A substrate for small patch antennas providing tunable miniaturization factors. *Microwave Theor Tech IEEE Transact.* 2006;54:135–146.

[4] SmithSchultz D, Markos SP, Soukoulis C. Determination of effective permittivity and permeability of metamaterials from reflection and transmission coefficients. *Phys Rev B.* 2002;65:195104.

[5] Yousefi L, Boybay MS, Ramahi OM. Characterization of metamaterials using a strip line fixture, antennas and propagation. *IEEE Transact.* 2011;59:1245–1253.

[6] Mookiah P, Dandekar KR. Metamaterial-substrate antenna array for MIMO communication system. *Antenna Propagat IEEE Transact.* 2009;57:3283–3292.

Resonant optical receiver design by series inductive peaking for sub-6 GHz RoF

L. Bogaert[1,2] | **J. Van Kerrebrouck**[1] | **A. Abbasi**[2] | **J. Lambrecht**[1] | **G. Torfs**[1] | **X. Yin**[1] | **G. Roelkens**[2] | **J. Bauwelinck**[1]

[1] Department of Information Technology (INTEC), IDLab Group, Ghent University–Imec, Ghent B-9052, Belgium

[2] Department of Information Technology (INTEC), Photonics Research Group, Ghent University–Imec, Ghent B-9052, Belgium

Correspondence
L. Bogaert, Department of Information Technology (INTEC), Ghent University, Ghent, Belgium.
Email: laurens.bogaert@ugent.be

Abstract

Future wireless communication links will require ever decreasing cell sizes to provide massive data capacity densities. Implementing a fully operational base station in each cell is not viable and thus centralized solutions making use of radio-over-fiber (RoF) have been proposed. Transimpedance amplifiers (TIAs) are an essential component in such RoF links. In this article, resonant TIAs making use of series inductive peaking are proposed for RoF communication links. Such a band-pass approach benefits from superior noise behavior and a relaxation of the transimpedance limit compared to the traditional broadband designs typically used in RoF.

KEYWORDS

Radio over Fiber, resonant receiver, series inductive peaking, transimpedance amplifier

1 | INTRODUCTION

The ever-increasing demand for high-speed wireless data connectivity requires new wireless network infrastructure. Part of the solution for this problem is shrinking the cell sizes. To make this a viable solution, the cost per remote antenna unit (RAU) has to decrease significantly. Radio-over-fiber (RoF,[1]) makes this decrease in cost per RAU possible by using a centralized approach hereby shifting the center of gravity from the RAU to the base station. In such a way resources can be shared between multiple RAUs.

Nowadays, RoF setups typically make use of broadband electronics and are thus not yet optimized for the intended radio schemes. In this article, we focus on optimizing the receiver side of the RAU by taking into account the narrowband nature of the signal. A design approach using series inductive peaking is proposed for implementing such a resonant transimpedance amplifier (TIA). Although broadband TIA requires a lowpass behavior with sufficient bandwidth (larger than the RF carrier used in the transmission scheme), a resonant TIA only needs sufficient gain in the targeted part of the spectrum. The devised TIA is not only superior in terms of noise behavior compared with a broadband TIA but is also capable of boosting the transimpedance. Whereas the first property can also be obtained by combining the broadband TIA with a band-pass filter, the second cannot.

The content of this article is subdivided in 2 main parts. First, the resonant design approach, analytic expressions describing its behavior and its advantages over traditional designs for radio schemes are discussed. Subsequently, a proof of concept is given for sub-6 GHz applications. Because of the limited bandwidth available at these lower frequencies, higher order modulation formats are typically used in sub-6 GHz applications with stringent requirements on the tolerated noise levels. For these types of applications, the noise performance can be largely improved by using a resonant TIA instead of a broadband TIA because RoF typically only targets a small fraction of the spectrum that is passed by a broadband TIA.

2 | MODELING OF THE PHOTODETECTOR

The proposed resonant TIA design process will depend heavily on the frequency dependent electrical behavior of the photodetector (PD) that is used. Since the frequency range of interest is rather small, a compact equivalent circuit (Figure 1) can already give a good fit between simulation and measurements.

The equivalent model (Figure 1) consists of 2 parts. The PD itself can be modeled[2] with a current source (I_{PD}), a junction capacitance (C_j), a shunt resistance (R_{sh}, which is typically negligible), and a series resistance. Secondly, the interconnect parasitics connecting the PD to the TIA are modeled as a series resistor-inductor element. This is possible because of the short interconnect length. The series resistance of the leads and the internal series resistance of the PD are combined in one parameter (R_s). The inductance of the leads is denoted by L_{lead}.

In case of a broadband design methodology, the tolerated amount of inductance is limited (although a very small inductance value might slightly increase the bandwidth without introducing peaking[3]). For passband applications, however, the presence of the lead inductor can be utilized to our advantage to introduce high-Q peaking and favor the transfer of the desired frequency band.

3 | TRANSIMPEDANCE

3.1 | Broadband TIA

The transimpedance (Z_T) of a broadband TIA (Figure 2) has a low-pass behavior (1) with 3 dB frequency $\omega_{0,BB}$ (2)[4]. These formulas were derived without taking R_{sh}, L_{lead}, and R_s into account and by using an amplifier with a frequency independent open loop voltage gain A. In these equations the parallel combination of the input capacitance of the TIA (C_{in}) and junction capacitance of the PD (C_j) is combined into the total capacitance C_T whereas R_F denotes the feedback resistance.
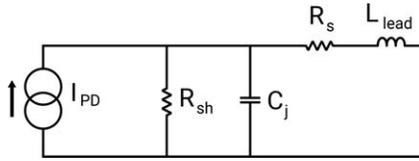
FIGURE 1 Equivalent network of a PIN PD

$$Z_T = -\frac{A}{A+1} R_F \frac{1}{1+\frac{s}{\omega_{0,BB}}} \quad (1)$$

$$\omega_{0,BB} = \frac{A+1}{R_F C_T} \quad (2)$$

This low-pass behavior, although desired for baseband signals, is not needed for RoF applications. Resonant TIA solutions make use of this extra degree of freedom by shaping the frequency dependent gain in such a way that it improves the signal-to-noise ratio (SNR) at the desired frequencies.

3.2 | Resonant TIA

The analytic expressions for the resonant TIA proposed in this article will be derived under the assumption of having sufficient loop gain at all frequencies of interest. Additionally, the goal is to size the amplifier and R_F in such a way that the input resistance R_{in} of the TIA (3)[4] is sufficiently smaller than the capacitive input impedance $|1/sC_{in}|$ of the TIA. If this condition is not fulfilled around the signal band, only a (possibly small) fraction of the useful R_F current going to the TIA will flow in the feedback path, resulting in inferior performances.

$$R_{in} \approx \frac{R_F}{A+1} \quad (3)$$

Under these assumptions, the transimpedance of the resonant receiver can be subdivided into 2 parts (4). The first part is the frequency dependent input circuitry, which will favor the desired frequency band by adopting series inductive peaking. Second, a current-to-voltage conversion is done through the feedback path of the TIA. This current-to-voltage conversion will by design ($1/\omega C_{in} \gg R_{in}$, and frequency independent A) be assumed to be approximately frequency flat for all frequencies of interest.

$$Z_T = \frac{I_{in}}{I_{PD}} \times \frac{V_{out}}{I_{in}} = \frac{I_{in}}{I_{PD}} \times -R_F \quad (4)$$

To calculate the frequency dependent filtering from I_{PD} to the current entering the TIA (I_{in}), the circuit depicted in Figure 1 is loaded by the input impedance of the TIA[4] (Figure 3). When sizing the circuit correctly, it is possible to initially neglect the input capacitance for all frequencies of interest. As discussed before, this is required to make sure

that most of the RF current I_{in} flows through the feedback path.

Biasing the TIA and PD independently will require the use of a decouple capacitor. Its value is typically chosen in such a way that it behaves as an RF short. In Figure 3, this DC-blocking capacitor was added explicitly to add extra tunability to the behavior of the input network.

Since we assume the current-to-voltage conversion from the input current I_{in} to the output voltage of the TIA to be nearly frequency flat for all frequencies of interest, the transfer function from the current generated in the PD (I_{PD}) to the current entering the TIA (I_{in}) will determine the frequency dependent behavior of the whole TIA.

The transfer function of the input network is easily obtained by observing that the circuit behaves as a current divider (5). The series combination of R_s and R_{in} is replaced by the total resistance R ($=R_s + R_{in}$) to get a more compact expression.

$$\frac{I_{in}}{I_{PD}} = \frac{1}{\left(1+\frac{C_j}{C_{block}}\right)+sR_T C_j + s^2 L_{lead} C_j} \quad (5)$$

When the decouple capacitor C_{block} is realized as an ideal DC block, the resonance (ie peaking) frequency ω_0 (6) of this second order low-pass transfer function will depend only on L_{lead} and C_j. Llead can be increased by adding an explicit inductance ($L_{explicit}$) in series with the original inductance, giving rise to a decrease in resonance frequency (7).

$$\omega_0\left(L_{explicit}=0, \ C_{block}=\infty\right) = \frac{1}{\sqrt{L_{lead} C_j}} \quad (6)$$

$$\omega_0\left(C_{block}=\infty\right) = \frac{1}{\sqrt{\left(L_{lead}+L_{explicit}\right)C_j}} \quad (7)$$

The disadvantage of using such a simple input circuit is that the product of L_{lead} and C_j will introduce an upper limit on the maximally achievable peaking frequency. This problem can be circumvented by using a finite value for C_{block} (8). The parameter α ($=\sqrt{1+C_j/C_{block}}$) was added to

FIGURE 2 Broadband TIA: general structure
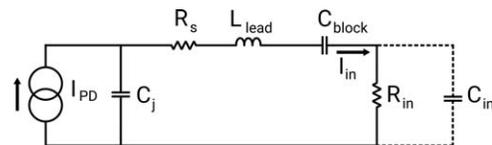
FIGURE 3 Input circuitry TIA: Series inductive peaking

describe the factor by which the resonance frequency is increased when using C_{block} with a finite value.

$$\omega_0 = \frac{\sqrt{1 + \frac{C_j}{C_{\text{block}}}}}{\sqrt{(L_{\text{lead}} + L_{\text{explicit}})C_j}} \triangleq \alpha \times \omega_0 (C_{\text{block}} = \infty) \qquad (8)$$

The peak height $|I_{\text{in}}(\omega_0)/I_{\text{in}}(0)|$ is denoted by the Quality (Q)-factor (9). This value will have a major impact on the performance improvement of the system. With respect to the noise behavior, it is advisable to work with a high Q-factor peak as it will boost the useful band relative to the broadband noise. However, it should be stressed that a higher Q also results in a lower signal bandwidth. Hence the Q-factor should be within certain bandwidth-determined boundaries. Consequently, the required bandwidth shall pose a limit to how much noise improvement we can expect by using this method. The available 3 dB (peaking) bandwidth $\Delta\omega$ (10)[5] is found to be inversely proportional to the Q-factor.

$$Q = \omega_0 \frac{L_{\text{lead}} + L_{\text{explicit}}}{R_T} = \frac{\alpha}{R_T}\sqrt{\frac{L_{\text{lead}} + L_{\text{explicit}}}{C_j}} \qquad (9)$$

$$\frac{\Delta\omega}{\omega_0} \approx \frac{1}{Q} \qquad (10)$$

4 | A PERFORMANCE COMPARISON BETWEEN RESONANT AND BROADBAND TIAS

When designing a TIA for RoF links, dedicated resonant TIA designs can result in superior performances. There are 3 main reasons to opt for such an approach.

First of all, higher center frequencies can be targeted by a resonant TIA. This is possible because of the fact that one can resonate parasitics out at any given frequency as long as the required component values exist for the given frequency range. Additionally, the bandwidth for such a resonant tank should be sufficiently high to pass the signal band. Because of the fact that the components used in the design are assumed to be fast enough, this property is not covered in this article but alternative resonant receiver topologies can be devised to benefit from this property when needed.

Second, the SNR can be boosted significantly by adopting such a method. This increases the spectral efficiency that can be obtained because higher order modulation formats can be adopted for similar error rates. This is the main reason why we introduced a resonant design because it will result in high data rates even for a limited bandwidth. This SNR improvement is a nice side effect caused by the peaking of the input circuitry at the carrier frequency. The improvements will be limited by the maximum Q value that can be obtained given a certain requirement on the signal
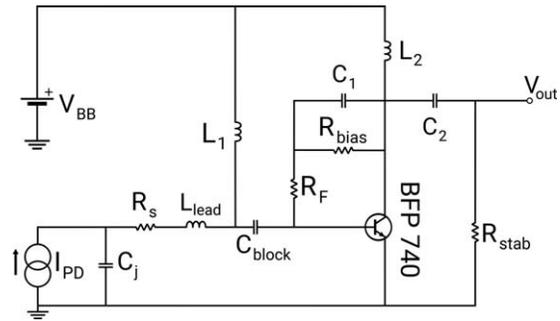
FIGURE 4 TIA design using series inductive peaking

bandwidth. However, the signal bandwidth for sub-6 GHz applications is typically limited since bandwidth is scarce and thus large sensitivity improvements can be expected by adopting series inductive peaking at the input.

A last advantage of this resonant technique is related to the limitation on the value that can be used for the feedback resistance (transimpedance limit,[6]) in broadband receivers. Consequently, there will be a limit to the output voltage. However, series inductive peaking at the input of the TIA boosts the transimpedance (11) and thus the output voltage. In Equation (11), $Z_{T,0}$ denotes the transimpedance at the resonance frequency (which is designed to coincide with the carrier frequency). The goal of the proposed resonant approach is to make sure that the SNR is significantly improved, resulting in $|Z_{T,0}| \gg R_F$.

$$Z_{T,0} = -R_F \times \frac{I_{\text{in}}}{I_{\text{PD}}}(f_0) = -R_F \times Q \times \frac{1}{\alpha^2} \qquad (11)$$

5 | PROPOSED TIA DESIGN: A PROOF OF CONCEPT

To illustrate the principle described in the previous section, a resonant TIA was designed with discrete components. For this proof-of-concept we targeted 150 MBaud communication of 64-QAM data modulated on a 4 GHz carrier. The proposed TIA design that makes use of series inductive peaking is given in Figure 4. This schematic includes the equivalent circuit of the PD (Figure 1) and the amplifier with feedback resistor R_F.

An RF choke L_1 (8 nH) is added to bias the PD whereas C_1 (1 nF), R_{bias} (51 kΩ) and L_2 (8 nH) are needed for obtaining the correct bias setting for the amplifier (where V_{BB} provides 4 V). The output part of the network consists of decouple capacitor C_2 (1 nF) and resistor R_{stab} (100 Ω). The latter is added to make the amplifier unconditionally stable.[7] Feedback resistance R_F (330 Ω) was chosen in function of the low-pass filtering introduced by the miller capacitance. Values for C_j (445 fF), R_s (7.09 Ω) and L_{lead} (3.85 nH) resulted from S-parameter measurements of the PD with the
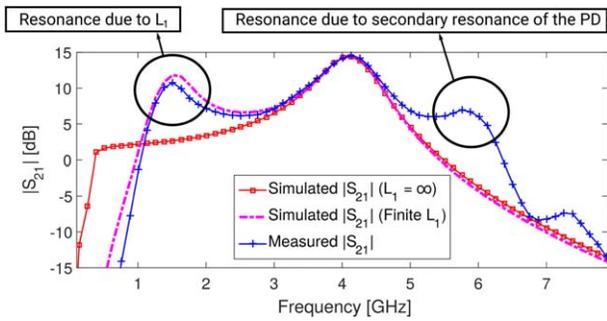
FIGURE 5 Measured S_{21} compared to simulated S_{21}. [Color figure can be viewed at wileyonlinelibrary.com]
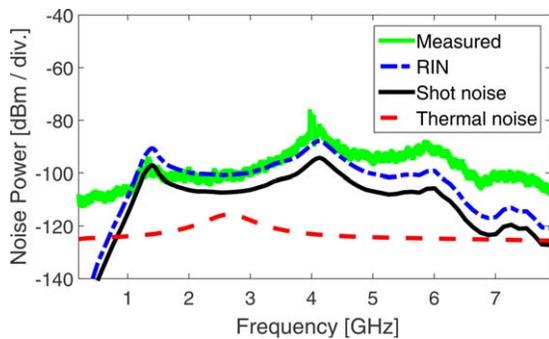
FIGURE 6 Noise contributions (Resolution bandwidth = 10 kHz). [Color figure can be viewed at wileyonlinelibrary.com]

required lead length. Equation (8) was then used to calculate the desired value for decouple capacitor C_{block} (1.5 pF).

5.1 | Transfer behavior

A link consisting of a distributed feedback (DFB) laser and the proposed resonant PD/TIA combination was used to test the transfer behavior (Figure 5). Frequency dependent effects of the laser were measured separately (with a high bandwidth photoreceiver) to compensate for the transmitter and make sure that the depicted transfer behavior only describes the PD/TIA combination rather than the whole link.

Simulations and measurements match very well for frequencies around the center frequency, over a range of nearly 2 GHz. However, an extra low frequency parasitic resonance is present that can be attributed to the fact that the RF choke L_1 (Figure 4) has a finite value. In future designs, this peak can be damped by adding a resistor in series to inductor L_1. Discrepancies at higher frequencies can be attributed to the fact that the models for the devices used are no longer adequate at these higher frequencies. The peak around 6 GHz is for example caused by a secondary resonance of the PD.

5.2 | Noise behavior

Using the same link as in the transfer function measurements, a 4 GHz sine wave is transmitted. The measured output spectrum shows not only the desired signal at the output but also a frequency dependent contribution of the noise (Figure 6) where the frequency dependence resembles the transfer function (Figure 5). It is important to remark that Figure 6 was constructed under the assumption of a frequency flat relative intensity noise (RIN) contribution. In practice, this is not the case and a maximum RIN contribution can be found close to the resonance frequency of the DFB laser (6 GHz for the given setup). This explains the discrepancy between the measured noise spectrum and the simulated noise spectrum. Noise shaping is clearly visible in the noise spectrum (Figure 6) and this is the result from adopting a resonant approach.

It can be seen that the RIN is the dominant noise effect for the given setup. Consequently, this link is not limited by the noise of the receiver. Nevertheless, the receiver will have a significant impact on how much the incoming noise deteriorates the signal. Using a resonant receiver will lower the noise contribution compared to a traditional broadband receiver, giving rise to an increase in SNR compared to a broadband TIA. This is caused by the fact that the RIN contribution experiences the previously mentioned noise shaping. The second most important noise contribution for the
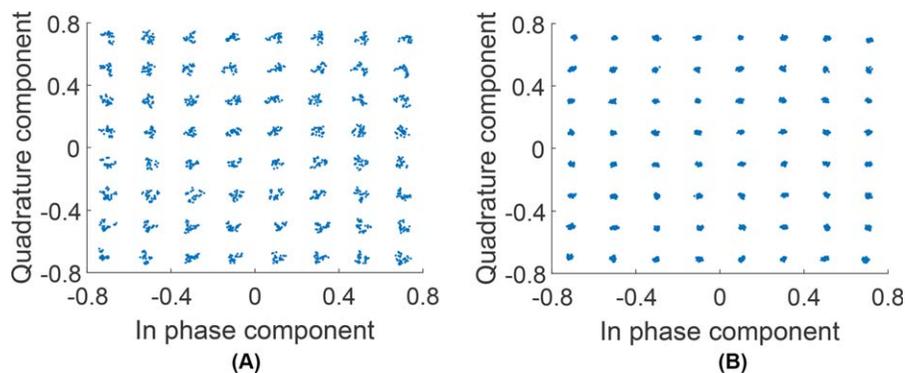
FIGURE 7 Constellation diagram: 64-QAM, 150 MBaud, 4 GHz carrier, root raised cosine filter (roll-off = 0.5) at receiver and transmitter (A) No equalization (B) 3 taps equalization. [Color figure can be viewed at wileyonlinelibrary.com]

given setup (shot noise, introduced by the PD) experiences the same noise shaping.

5.3 | Constellation diagram

Nearly the same link was used to do the communication tests. The only difference is that a 10 dB optical attenuator was added in between the DFB laser and the PD/TIA combination to lower the RIN and shot noise. The output of the resonant receiver was then sensed by a real-time scope (Figure 7). It is shown in Figure. 7 that when a limited amount of equalization taps (3 taps) is added at the receiver, error-free (SNR = 35.8 dB) 900 Mbps communication can easily be provided over an RoF link with a symbol rate of 150 MBaud.

6 | ESSENTIAL RoF SPECIFICATIONS: A CONCLUSION

In the context of RoF links, there are several important specifications for the RAUs. Noise will be key in RoF to be able to transfer high order modulation formats. Traditional RAUs are, however, not yet optimized for the radio schemes used in RoF links and this article addresses this shortcoming by adopting a resonant design approach for the RAU receiver.

Furthermore, a massive amount of RAUs will be deployed in the case of 5G. Consequently, the cost, power consumption and occupied surface area should be small enough to make this technology scalable for 5G. The resonant TIA designed as a proof of concept has a footprint of 1.1 cm × 1 cm and consumes 73.5 mW of power, which can be further optimized by integration on chip.

REFERENCES

[1] Thomas V, El-Hajjar AM, Hanzo L. Performance improvement and cost reduction techniques for radio over fiber communications. *IEEE Commun. Surveys Tuts.* 2015;17(2):627–670.

[2] Urick VJ, Williams KJ, McKinney JD. *Fundamentals of Microwave Photonics*. Wiley; Hoboken, NJ, 2015: 25–26.

[3] Neuhauser M, Rein HM, Wernz H. Low-Noise, High-Gain Si-Bipolar Preamplifiers for 10 Gb/s Optical-fiber links – Design and Realization. *IEEE J Solid-State Circuits.* 1996;31(1):24–29.

[4] Säckinger E. *Broadband Circuits for Optical Fiber Communication*. Wiley; Hoboken, NJ, 2005: 113–114.

[5] DunnRossing FT, Hartmann WM, Campbell DM, Fletcher NH. *Springer Handbook of Acoustics*. 2nd ed. Springer; 2015: 532.

[6] Säckinger E. The transimpedance limit. *IEEE Trans Circuits Syst I, Reg Papers.* 2010;57(8):1848–1856.

[7] Pozar DM. *Microwave Engineering*. 2nd ed. Wiley; Hoboken, NJ, 1997: 612–622.

Frequency and pattern reconfigurable saline-water antenna array

Ren-Gui Fan | Ya-Hui Qian | Qing-Xin Chu (iD)

School of Electronic and Information Engineering, South China University of Technology, Guangzhou, Guangdong, People's Republic of China

Correspondence
Qing-Xin Chu, School of Electronic and Information Engineering, South China University of Technology, Guangzhou, Guangdong, China.
Email: qxchu@scut.edu.cn

Abstract

A saline-water monopole antenna array is proposed in this article. The saline-water monopole antenna consists of a feeding probe and a saline-water cylinder held by a polyvinyl chloride tube. The feeding probe is loaded with a mental disk on the top to improve the excitation of TM mode, and there is a teflon base between the water and ground to maximize the bandwidth. The saline-water monopole antenna is placed in the middle of the ground, around which, four parasitic saline-water monopoles are symmetrically placed so that a cross-shaped saline-water monopole antenna array is formed. By controlling the injection of the water and the heights of the water cylinders, the antenna array achieves reconfigurable frequencies and patterns with high efficiency. The commercial software ANSYS HFSS is used for the antenna modeling and simulation. The final design is fabricated and tested. A good agreement is obtained between the simulation and measurement results.